

Fusion hindrance for $^{58}\text{Ni} + ^{54}\text{Fe}$ A. M. Stefanini,¹ G. Montagnoli,² L. Corradi,¹ S. Courtin,³ E. Fioretto,¹ A. Goasduff,³ F. Haas,³ P. Mason,² R. Silvestri,¹ Pushendra P. Singh,¹ F. Scarlassara,² and S. Szilner⁴¹*Istituto Nazionale di Fisica Nucleare, Laboratori Nazionali di Legnaro, I-35020 Legnaro (Padova), Italy*²*Dipartimento di Fisica, Università di Padova, and Istituto Nazionale di Fisica Nucleare, Sezione di Padova, I-35131 Padova, Italy*³*Institut Pluridisciplinaire Hubert Curien, Centre National de la Recherche Scientifique-Institut National de Physique Nucleaire et de Physique des Particules, Université de Strasbourg, F-67037 Strasbourg Cedex 2, France*⁴*Ruder Bošković Institute, HR-10002 Zagreb, Croatia*

(Received 8 May 2010; published 26 July 2010)

The fusion excitation function of $^{58}\text{Ni} + ^{54}\text{Fe}$ has been measured in a cross-section range from $\simeq 1 \mu\text{b}$ up to around 450 mb. Coupled-channels calculations, using a standard Woods-Saxon ion-ion potential, reproduce the excitation function down to about $180 \mu\text{b}$. At lower energies, fusion cross sections drop faster than calculations, with a steep slope. The astrophysical S factor shows a maximum at the lowest energies. These results are compared with various evidence from recent experiments on other systems with projectile and target in the mass range $A \simeq 30\text{--}60$.

DOI: [10.1103/PhysRevC.82.014614](https://doi.org/10.1103/PhysRevC.82.014614)

PACS number(s): 25.70.Jj, 24.10.Eq

I. INTRODUCTION

Heavy-ion fusion cross sections in the vicinity of the Coulomb barrier are mainly determined by couplings of the relative motion of the two colliding nuclei to their low-energy surface vibrations and/or stable deformations [1,2]. Nucleon transfer channels play a concurring role in several cases. Multiphonon excitations have been shown [3] to become important for medium-heavy nuclei and produce complex fusion barrier distributions with discrete structures [4,5]. Below the lower energy limit of such distributions, an interesting trend was discovered in recent years [6]: The fusion excitation function shows a sharp decrease with decreasing energy, well below the expectations based on standard coupled-channels (CC) calculations. This evidence was named “fusion hindrance,” an expression which actually covers a wide range of behaviors for different mass ranges and different nuclear-structure situations. Clearing up the underlying physics is presently a major goal of a variety of studies in the field of low-energy heavy-ion reaction dynamics [1]. Various experimental evidence has been reported, together with model calculations [7–10], in an effort to understand the fusion hindrance phenomenon. Discussions in this respect are lively in the low-energy heavy-ion physics community, especially for medium-light systems where the trend of the sub-barrier fusion cross sections has been shown either to strongly differ or to show striking similarities in nearby systems.

Measurements have been performed for the systems $^{36}\text{S} + ^{48}\text{Ca}$ [11] and $^{48}\text{Ca} + ^{48}\text{Ca}$ [12] in recent years. The two excitation functions decrease regularly down to the submicrobarn level, showing remarkably parallel behavior. In more detail, the two logarithmic derivatives $L(E) = d[\ln(\sigma E)]/dE$, after a sharp (expected) increase just below the Coulomb barrier, level off and become pretty constant with decreasing cross section as a function of the energy. The Q value for compound nucleus formation has opposite signs for $^{36}\text{S} + ^{48}\text{Ca}$ and $^{48}\text{Ca} + ^{48}\text{Ca}$ ($Q = +7.6 \text{ MeV}$ and $Q = -3.0 \text{ MeV}$, respectively). It was thus concluded that the sign of the Q value is irrelevant in the

measured energy range. Analogously, for the positive Q -value system $^{27}\text{Al} + ^{45}\text{Sc}$ [13], the cross sections drop much below the results of standard CC calculations, even if in this system (and in various others with $Q > 0$) no clear evidence could be extracted for a maximum of the astrophysical S factor [14,15] as a function of the energy [$S(E) = \sigma E \exp(2\pi\eta)$].

On the other hand, in the (slightly) heavier systems $^{58}\text{Ni} + ^{58}\text{Ni}$ [16] and $^{64}\text{Ni} + ^{64}\text{Ni}$ [17], the logarithmic slopes keep increasing down to very low energies. They reach and overcome the value (L_{CS}) corresponding to a constant S factor. One faces the problem of understanding the blend of reaction dynamics and nuclear structure producing these unsystematic behaviors, when comparing the slopes of Ni + Ni and lighter systems.

This prompted us to measure near- and sub-barrier fusion cross sections for the intermediate case $^{58}\text{Ni} + ^{54}\text{Fe}$. Here the low-energy quadrupole and octupole excitations have similar excitation energies and strengths for projectile and target. Thus, the near-barrier excitation function (and the fusion barrier distribution where available) are expected to differ only slightly from Ni + Ni systems. This has been experimentally verified by comparison with $^{58}\text{Ni} + ^{58,60}\text{Ni}$ and was the subject of a recent brief paper [18].

However, given the present incomplete understanding of the fusion hindrance phenomenon, $^{58}\text{Ni} + ^{54}\text{Fe}$ and the various Ni + Ni systems might show different trends well below the barrier, that is, below the lowest energy peak of the barrier distribution, where the effects of channel couplings effectively vanish. In particular, we need to check whether the slope of the excitation function saturates (as, e.g., for $^{48}\text{Ca} + ^{48}\text{Ca}$) or keeps increasing with decreasing energy (as, e.g., for $^{58}\text{Ni} + ^{58}\text{Ni}$) in the perspective of further theoretical analyses of fusion hindrance for such medium-light systems.

We have measured the excitation function for $^{58}\text{Ni} + ^{54}\text{Fe}$ down to very small cross sections, and this article reports in some detail the results of the whole experiment. The description of the setup and procedures (Sec. II) is followed by the presentation of the results in Sec. III. Then CC calculations

TABLE I. Fusion cross sections of $^{58}\text{Ni} + ^{54}\text{Fe}$. Quoted errors are statistical uncertainties only.

$E_{c.m.}$ (MeV)	σ_{ER} (mb)	$E_{c.m.}$ (MeV)	σ_{ER} (mb)
85.36	0.0011 ± 0.00079	95.97	116.8 ± 1.8
85.84	0.0022 ± 0.0010	96.93	132.9 ± 3.0
86.32	0.0139 ± 0.0035	97.90	167.1 ± 3.7
86.81	0.0358 ± 0.0049	98.86	198.1 ± 4.3
87.29	0.178 ± 0.019	99.82	219.5 ± 3.7
88.25	0.795 ± 0.070	100.79	250.5 ± 3.5
89.22	3.91 ± 0.12	101.75	276.1 ± 4.7
90.18	8.61 ± 0.21	103.68	332.5 ± 8.7
91.14	15.93 ± 0.34	104.65	357.4 ± 8.4
92.11	27.46 ± 0.61	106.57	390.7 ± 6.2
93.07	46.73 ± 0.86	107.54	418.2 ± 7.1
94.04	64.48 ± 1.44	109.47	435.1 ± 5.0
95.00	85.61 ± 1.91		

are introduced and discussed in Sec. IV. Section V summarizes and concludes this work.

II. THE SETUP

The XTU Tandem accelerator of the Laboratori Nazionali di Legnaro of Istituto Nazionale di Fisica Nucleare (INFN) provided ^{58}Ni beams in the energy range 178–228 MeV, with intensities of $\simeq 5\text{--}8$ pA. The targets were installed in a sliding-seal scattering chamber and consisted of $40 \mu\text{g}/\text{cm}^2$ metallic iron evaporations on a $15\text{-}\mu\text{g}/\text{cm}^2$ carbon backing facing the beam. The isotopic compositions of the targets were 99.915%, 0.06%, 0.02%, and $<0.0005\%$ for $^{54,56,57,58}\text{Fe}$, respectively. The small amounts of iron isotopes heavier than $A = 54$ led to very small corrections to the measured fusion ER yields near and above the barrier but actually prevented measuring fusion cross sections smaller than $\simeq 1 \mu\text{b}$. The beam energy loss across the carbon backing and half of the ^{54}Fe target was $\simeq 950$ keV, depending on the energy, and it was taken into account in the data reduction. The energies listed in Table I are corrected values.

The ERs were detected by using the setup (see also Ref. [18]) schematically shown in Fig. 1. The ERs were separated from the beam in the electrostatic deflector [19]. Subsequently, they were detected by two microchannel plate detectors (MCP1 and MCP2), entered a transverse-field

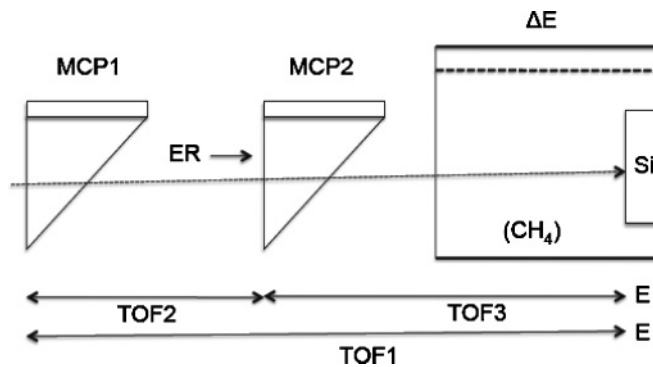


FIG. 1. The experimental detector setup following the electrostatic beam separator.

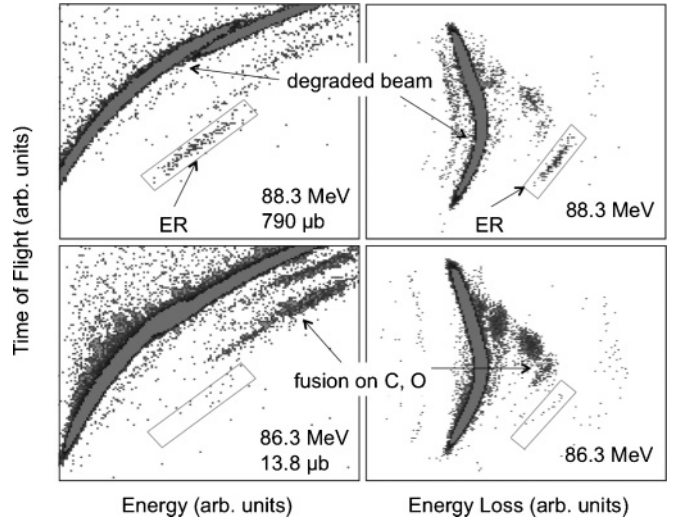


FIG. 2. Two-dimensional spectra of time-of-flight (TOF2) vs. total energy E and energy loss ΔE measured in the present experiment (see Ref. [11] for comparison). The group of evaporation residues (ERs) is clearly seen at the higher energy, 88.3 MeV (two upper panels). At the lower energy, 86.3 MeV, ERs are better identified in the TOF2 vs. ΔE representation than in the TOF2 vs. E matrix (two lower panels). The rectangles enclosing the ER at 88.3 MeV are reported on the spectra at 86.3 MeV and were used to count the fusion events for this and other low energies, with the further condition that the events must exist in both representations (TOF2 vs. E and TOF2 vs. ΔE) at the same TOF2 channel. The two other TOF signals, TOF1 and TOF3, were used for checking the results.

ionization chamber (IC) giving an energy loss (ΔE) signal, and finally stopped in a circular 2000-mm² silicon detector placed in the same gas (CH_4) volume. The silicon detector provided the residual energy E_R , as well as the starting signal used for the TOF1, TOF2, TOF3, and triggered the data acquisition. The total length of the detector telescope was $\simeq 105$ cm with a geometrical solid angle of 0.171 ± 0.003 msr (limited by the silicon detector size).

This detector setup improves the one we used in recent experiments [11,12], where the IC was not installed. The additional ΔE signal provided by the IC was a valuable tool for ER identification, especially at very low energies. Inspection of the spectra shown in Fig. 2 allows one to appreciate the advantage. Four silicon detectors were used for beam control and normalization between the different runs by measuring the Rutherford scattering from the target. They were placed above and below and to the left and right of the beam at the same scattering angle, $\theta_{\text{lab}} = 16^\circ$. The solid angle of all detectors, including the E - ΔE -TOF telescope, was determined by placing an α source at the target position.

ER angular distributions were measured at $E_{\text{lab}} = 192$ and 206 MeV in the range 0° to 7° [18]. Total fusion cross sections were derived by integrating such distributions and by a simple inter(extra)polation procedure for all other energies where ER measurements were taken only at 0° (2° for low energies). Furthermore, the absolute cross sections rely on the knowledge of the relevant solid angles and the transmission efficiency of the electrostatic deflector. This transmission was measured

by detecting ER at 3° after switching off the deflector, then by comparing their yields with the results of the analogous measurement with the beam deflector on. The resulting value of the transmission is $T = 0.78 \pm 0.03$.

Systematic errors on the absolute cross-section scale sum up to an estimated $\pm 7\%$, due to the geometrical solid-angle uncertainties, the angular distribution integrations, and the transmission measurement. Relative errors are essentially determined by statistical uncertainties which do not exceed 2–3% near and above the barrier but become much larger, and dominate, at low energies where few fusion events could be detected. At the lowest energy, only two ERs were unambiguously identified in a sequence of four $\simeq 6$ -h runs.

III. RESULTS AND EXPERIMENTAL TRENDS

The measured fusion excitation function is shown in Fig. 3 in logarithmic and linear scales (upper and lower panels, respectively). The cross sections are also listed in Table I. They range from $\simeq 1 \mu\text{b}$ to more than 400 mb. Above the barrier, the trend is very regular, but this is not the case below the barrier (the Coulomb barrier obtained by the widely used

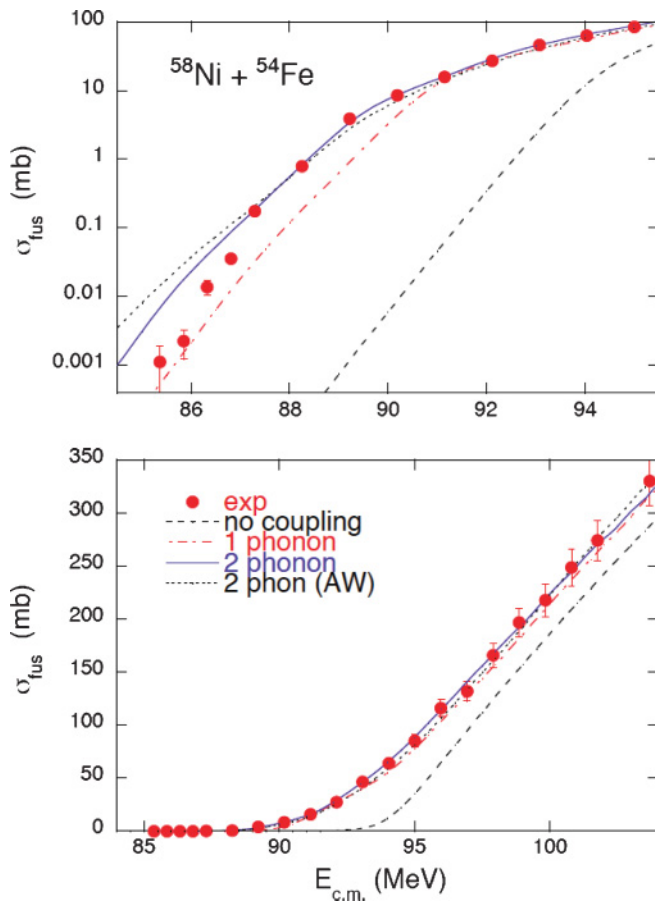


FIG. 3. (Color online) The excitation function of $^{58}\text{Ni} + ^{54}\text{Fe}$ measured in this work is compared with the results of various CC calculations discussed in the text. Total errors (statistical plus systematic ones) are plotted in the bottom panel. Only statistical uncertainties are reported in the top panel.

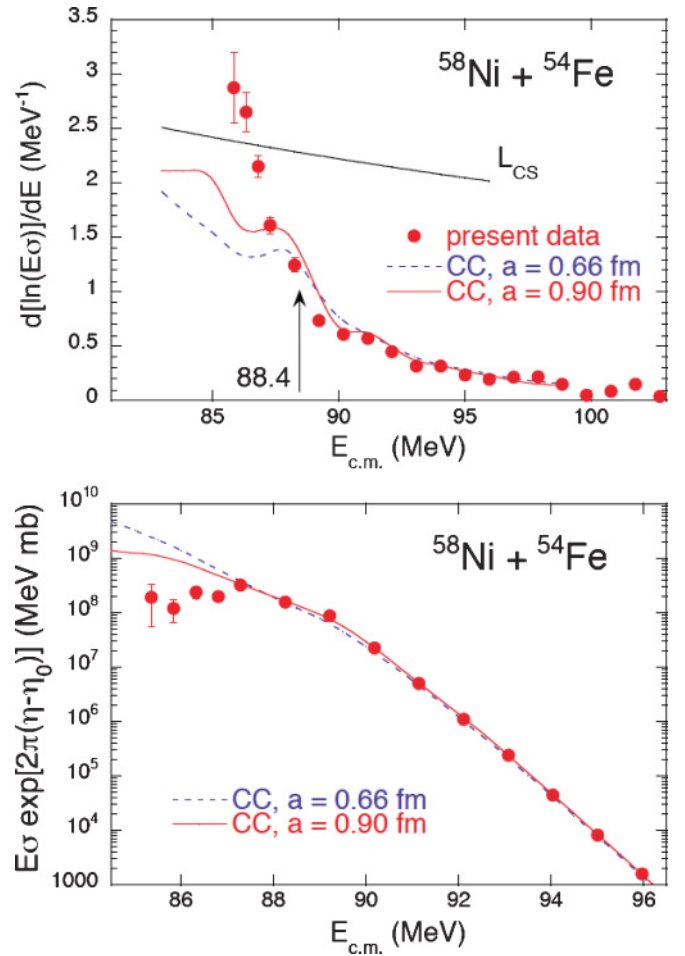


FIG. 4. (Color online) (Top) Logarithmic derivative of $E\sigma$ with respect to the energy. It is obtained as the incremental ratio for successive pairs of experimental points. The cross section measured at the lowest energy (85.36 MeV) was not used, because of its very large uncertainty (see Table I). (Bottom) S factor vs. energy derived from the present data. In the S plot, a η_0 value of 62.00 has been used for easy visualization.

Akyüz-Winther potential [20] is around 93 MeV). One can better appreciate the behavior below the barrier in the plot shown in Fig. 4 (top panel). Here, the logarithmic derivative (slope) of the excitation function is reported versus the energy. This slope keeps increasing with decreasing energy down to the lowest measured E . It clearly reaches and overcomes L_{CS} at $E = E_{CS} \simeq 86.7$ MeV. This energy marks an experimental threshold for hindrance. The S factor develops a maximum (bottom panel) at that energy, as expected. The existence of this S factor maximum is quite clear.

The very regular increase of the slope for the present system, $^{58}\text{Ni} + ^{54}\text{Fe}$, can be contrasted with the behavior observed for $^{48}\text{Ca} + ^{48}\text{Ca}$ [12], where the slope does increase below the barrier, but a saturation shows up before reaching L_{CS} and the slope tends to become parallel to L_{CS} with further decreasing energy. This can be appreciated from Fig. 5, where the behavior of the slope for these two systems is reported. The case of $^{58}\text{Ni} + ^{58}\text{Ni}$ [16], where a clear-cut hindrance was observed, is also plotted for comparison. The trend of $^{58}\text{Ni} + ^{54}\text{Fe}$ we

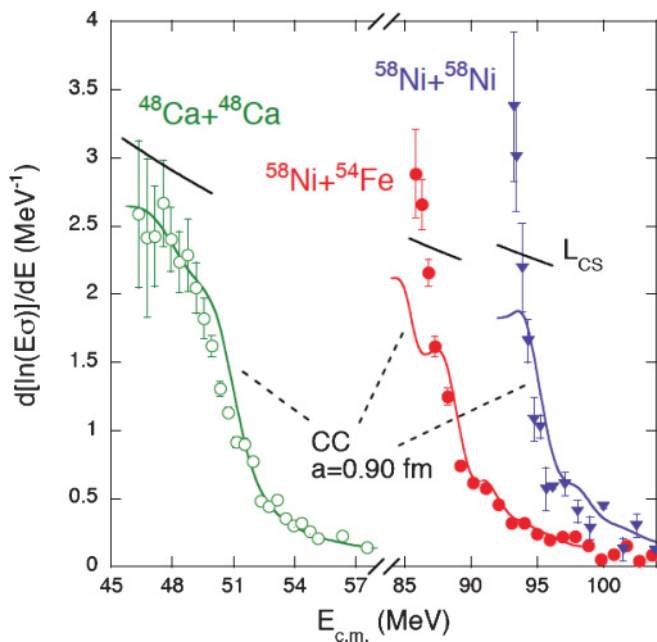


FIG. 5. (Color online) Logarithmic slopes of fusion excitation functions of $^{58}\text{Ni} + ^{54}\text{Fe}$, $^{58}\text{Ni} + ^{58}\text{Ni}$, and $^{48}\text{Ca} + ^{48}\text{Ca}$ in a common energy scale. Quoted errors are only statistical.

observe in the present measurements closely resembles that of $^{58}\text{Ni} + ^{58}\text{Ni}$.

Extracting fusion barrier distributions from the second energy derivative of the fusion excitation function [4] is in general of great help in understanding the kind of couplings involved in fusion reactions near the barrier. However, at deep subbarrier energies, the trend of the logarithmic derivative of the excitation function becomes a more sensitive tool for such analyses. This follows from the simple relation [6] between the barrier distribution $\text{BD}(E)$ and the logarithmic derivative (slope) $L(E)$

$$\text{BD}(E) = \sigma E \left[\frac{dL(E)}{dE} + [L(E)]^2 \right]. \quad (1)$$

The term $L(E)^2$ and the overall factor σE hide any irregularity of the slope in the barrier distribution. Recently [21], this concept has been applied to the case of fusion of calcium isotopes: While the logarithmic derivative of $^{48}\text{Ca} + ^{48}\text{Ca}$ has the intriguing behavior mentioned here, it is impossible to recognize any structure at low energies below the main peak [12] of the barrier distribution.

The barrier distribution we have extracted from the data for $^{58}\text{Ni} + ^{54}\text{Fe}$ is reported in Fig. 6 in a logarithmic scale. The distribution has been obtained [4] by double differentiation of $E\sigma_{\text{fus}}$ with respect to the energy, using the three-point difference formula [22] with an energy step $\Delta E \simeq 2$ MeV (3 MeV above 95.5 MeV). Its complex shape results from couplings to multiphonon states [18]. From Fig. 6, it is straightforward to estimate that the lowest barrier is around 88.4 MeV. Of course, due to the smoothing introduced by quantal barrier penetration [4], we observe an effective continuous distribution replacing the set of discrete barriers produced by couplings and extending below 88.4 MeV. If we

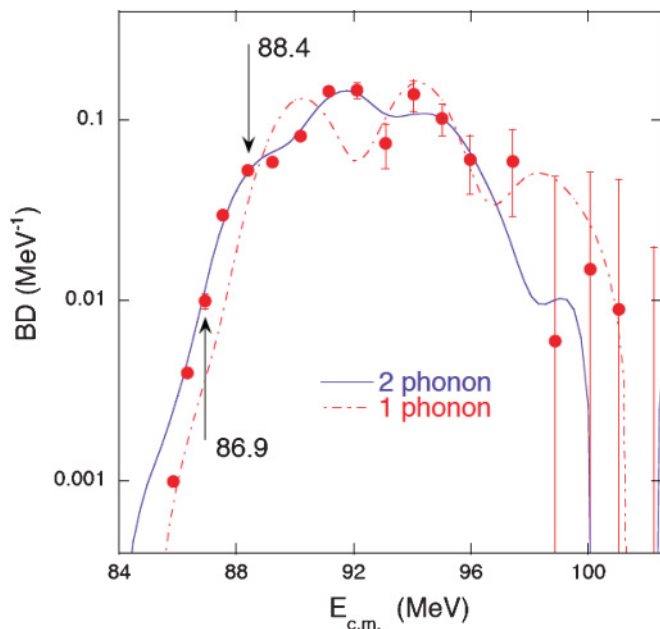


FIG. 6. (Color online) The barrier distribution extracted from the data in a logarithmic scale vs. energy. The distribution is normalized to one. The arrows mark the two energies commented in the text.

choose to (arbitrarily) define the lower limit of the distribution as the energy E_{BD} where it is 0.01 MeV^{-1} , it follows that $E_{\text{BD}} \simeq 86.9 \text{ MeV}$, which is quite close to E_{CS} . In other words, fusion hindrance shows up just below the energy where the barrier distribution vanishes. This is not a new finding, but it is particularly evident in the present system and tells us that no weak low-energy barrier exists, even though that would be very hard to discern in the barrier distribution.

We notice that, prior to the present measurement on $^{58}\text{Ni} + ^{54}\text{Fe}$, only for $^{32,34}\text{S} + ^{89}\text{Y}$ could a well-defined barrier distribution [23] and a clear maximum of the S factor [17] be extracted from the measured fusion excitation function. Like for $^{58}\text{Ni} + ^{54}\text{Fe}$, in those two cases, the S factor maximum (at E_{CS}) develops very close to the low-energy limit E_{BD} of the barrier distribution.

IV. ANALYSIS AND DISCUSSION

We have chosen to analyze the present data with the CC code CCFULL [24]. A rather complete description of the calculations can be found in Ref. [18], and here we only recall their main features. One knows that CCFULL may be inadequate, in particular as far as the Woods-Saxon (WS) parametrization of the ion-ion potential is concerned, to give account of the fusion cross sections at very low energies. This was pointed out in recent years [6–12]; however, this kind of standard CC analysis shows the basic trends of the low-energy cross sections and helps put the data in a reference frame that can be a convenient starting point for further theoretical treatments.

The low-lying quadrupole vibrations have roughly equal excitation energies and strengths in ^{58}Ni and ^{54}Fe (1.454 and 1.408 MeV, with $\beta_2 = 0.18$ and 0.20, respectively). In both cases, the octupole states lie above 4 MeV and are weak, so

TABLE II. Parameters of the WS potentials used in the CC calculations.

	$V_o(\text{MeV})$	a (fm)	r_o (fm)
AW	81.2	0.67	1.15
CC	107.2	0.90	1.05

that they have a nearly adiabatic influence on the dynamics, that is, lowering the barrier (i.e., enhancing fusion cross sections for a given energy) with little effect on the shape of the barrier distribution.

The CC calculations shown in Figs. 3 and 4 used the same two ion-ion potentials of Ref. [18] where the purpose was to reproduce the details of the excitation function near and slightly below the barrier. The parameters of the two WS potentials are specified in Table II. Both of them produce a barrier, $V_b = 94.0$ MeV, that is, 1.3 MeV higher than the Akyüz-Winther (AW) barrier [20].

The potential labeled “AW” in Table II differs only slightly from the AW potential. Small variations of the radius parameter and of the potential well have been calculated, with the purpose of obtaining a good fit of the cross sections at above-barrier energies and of the centroid of the experimental barrier distribution. The other potential (CC) in Table II has been constructed by imposing a larger diffuseness, $a = 0.90$ fm, and then adjusting the radius parameter and the depth of the well to achieve the same barrier height. With respect to the standard AW geometry, with $a = 0.67$ fm in this case, a more diffuse WS potential simulates a fusion hindrance, since it produces a thicker barrier, leading to a steeper decrease of the excitation function at low energies.

The results of the CC analysis are reported in Figs. 3, 4, and 6. As in Ref. [18], the one-phonon calculation includes one octupole phonon and one quadrupole phonon in both projectile and target, as well as the mutual excitation of such states. Analogously, two quadrupole phonons and all possible mutual excitations were included in the so-called two-phonon calculation. Both two-phonon calculations are able to fit the data down to about 0.1 mb (see Fig. 3). Further below the barrier, the slope is not reproduced either with $a = 0.67$ fm or with $a = 0.90$ fm, even if this last calculation gets nearer to the data (see also Fig. 4). It appears that one should use a still larger diffuseness to follow the steep decrease of the fusion cross sections below ≈ 87 MeV. Indeed, we have pointed out before that around this energy the slope reaches L_{CS} ($E_{CS} = 86.7$ MeV) and the barrier distribution terminates ($E_{BD} = 86.9$ MeV). Still, this distribution is nicely reproduced by the two-phonon calculation either with $a = 0.67$ fm or with $a = 0.90$ fm [18]. This indicates once more that the barrier distribution is not a sensitive tool to reveal details of the excitation function at deep sub-barrier energies (see Sec. III).

Figure 5 shows again the slope obtained with $a = 0.90$ fm, together with analogous calculations for $^{58}\text{Ni} + ^{58}\text{Ni}$ and for $^{48}\text{Ca} + ^{48}\text{Ca}$ (taken from Ref. [12]), whose flattened slope is fit using that large diffuseness.

V. SUMMARY AND CONCLUSIONS

This article has reported on the measurement of the fusion excitation function for the system $^{58}\text{Ni} + ^{54}\text{Fe}$ in a wide energy range from well above to well below the Coulomb barrier, down to ≈ 1 μb . In particular, the trend of the sub-barrier excitation function has been discussed in detail. The cross sections decrease very steeply at the lowest energies, and the logarithmic slope of the excitation function keeps increasing to reach and overcome the value L_{CS} expected for a constant astrophysical S factor. Consequently, this shows a clear maximum as a function of the energy.

CC calculations, using a standard WS ion-ion potential, give a good account of the excitation function only down to about 180 μb . At lower energies, fusion cross sections drop faster than calculations and might only be reproduced by calculations employing a very large and unrealistic diffuseness of the ion-ion potential with WS shape. A “fusion hindrance” is quite clear in the present system. The threshold energy for this behavior may be estimated from (1) where the logarithmic slope reaches L_{CS} , (2) where the extracted barrier distribution vanishes, and (3) where standard CC calculations start overestimating the cross sections. These three energies are very near to each other (the average value is $\approx 86.8 \pm 0.2$ MeV) and fall slightly above the value (83.8 MeV) expected from the phenomenological systematics of Jiang *et al.* [13].

Fusion of $^{58}\text{Ni} + ^{54}\text{Fe}$ at low energies resembles the trend observed for Ni + Ni systems [17] and is different from what is observed for $^{48}\text{Ca} + ^{48}\text{Ca}$ [12] (and for $^{36}\text{S} + ^{48}\text{Ca}$ [11]) where the slope almost saturates below L_{CS} . Rather than from the shape of the barrier distribution, the low-energy behavior of all these systems is best revealed by the trend of the logarithmic slope, as pointed out recently [21]. Further theoretical analyses are required to disentangle the mixture of nuclear structure and dynamics producing these unsystematic trends.

ACKNOWLEDGMENTS

We thank C. L. Jiang for useful discussions and a critical reading of the manuscript. We are very grateful to the XTU Tandem staff and to M. Loriggiola for preparing targets of excellent quality. This work was partially supported by the European Commission within the Sixth Framework Programme through I3-EURONS (Contract No. RII3-CT-2004-506065) and by the Croatian Grant MZOS 0098-1191005-2890.

[1] Proc. Int. Conf. on “New Aspects of Heavy Ion Collisions Near the Coulomb Barrier,” Fusion08, Chicago, Illinois, 22–26 September 2008, AIP Conf. Proc. 1098, edited by K. E. Rehm, B. B. Back, H. Esbensen, and C. J. Lister (AIP, Melville, NY, 2009).

[2] M. Dasgupta, D. J. Hinde, N. Rowley, and A. M. Stefanini, *Annu. Rev. Nucl. Part. Sci.* **48**, 401 (1998).

[3] H. Esbensen, *Phys. Rev. C* **72**, 054607 (2005).

[4] N. Rowley, G. R. Satchler, and P. H. Stelson, *Phys. Lett. B* **254**, 25 (1991).

- [5] A. M. Stefanini *et al.*, *Phys. Rev. Lett.* **74**, 864 (1995).
- [6] C. L. Jiang *et al.*, *Phys. Rev. Lett.* **89**, 052701 (2002).
- [7] Ş. Mişicu and H. Esbensen, *Phys. Rev. C* **75**, 034606 (2007).
- [8] H. Esbensen and Ş. Mişicu, *Phys. Rev. C* **76**, 054609 (2007).
- [9] A. Diaz-Torres, D. J. Hinde, M. Dasgupta, G. J. Milburn, and J. A. Tostevin, *Phys. Rev. C* **78**, 064604 (2008).
- [10] T. Ichikawa, K. Hagino, and A. Iwamoto, *Phys. Rev. Lett.* **103**, 202701 (2009).
- [11] A. M. Stefanini *et al.*, *Phys. Rev. C* **78**, 044607 (2008).
- [12] A. M. Stefanini *et al.*, *Phys. Lett. B* **679**, 95 (2009).
- [13] C. L. Jiang *et al.*, *Phys. Rev. C* **81**, 024611 (2010).
- [14] C. L. Jiang, H. Esbensen, B. B. Back, R. V. F. Janssens, and K. E. Rehm, *Phys. Rev. C* **69**, 014604 (2004).
- [15] E. M. Burbidge, G. R. Burbidge, W. A. Fowler, and F. Hoyle, *Rev. Mod. Phys.* **29**, 547 (1957).
- [16] M. Beckerman, J. Ball, H. Enge, M. Salomaa, A. Sperduto, S. Gazes, A. DiRienzo, and J. D. Molitoris, *Phys. Rev. C* **23**, 1581 (1981).
- [17] C. L. Jiang *et al.*, *Phys. Rev. Lett.* **93**, 012701 (2004).
- [18] A. M. Stefanini *et al.*, *Phys. Rev. C* **81**, 037601 (2010).
- [19] S. Beghini, C. Signorini, S. Lunardi, M. Morando, G. Fortuna, A. M. Stefanini, W. Meczynski, and R. Pengo, *Nucl. Instrum. Methods A* **239**, 585 (1985).
- [20] Ö. Akyüz and Å. Winther, in *Nuclear Structure and Heavy-Ion Physics, Proceedings of the International School of Physics "Enrico Fermi," Course LXXVII, Varenna*, edited by R. A. Broglia and R. A. Ricci (North Holland, Amsterdam, 1981).
- [21] N. Rowley and K. Hagino, *Nucl. Phys. A* **834**, 110C (2010).
- [22] H. Timmers, L. Corradi, A. M. Stefanini, D. Ackermann, J. H. He, S. Beghini, G. Montagnoli, F. Scarlassara, G. F. Segato, and N. Rowley, *Phys. Lett. B* **399**, 35 (1997); H. Timmers, D. Ackermann, S. Beghini, L. Corradi, J. H. He, G. Montagnoli, F. Scarlassara, A. M. Stefanini, and N. Rowley, *Nucl. Phys. A* **633**, 421 (1998).
- [23] A. Mukherjee, M. Dasgupta, D. J. Hinde, K. Hagino, J. R. Leigh, J. C. Mein, C. R. Morton, J. O. Newton, and H. Timmers, *Phys. Rev. C* **66**, 034607 (2002).
- [24] K. Hagino, N. Rowley, and A. T. Kruppa, *Comput. Phys. Commun.* **123**, 143 (1999).